# Cdk5-dependent phosphorylation of liprinα1 mediates neuronal activity-dependent synapse development

Huiqian Huang[a,b,c,1], Xiaochen Lin[a,b,c], Zhuoyi Liang[a,b,c], Teng Zhao[d], Shengwang Du[d], Michael M. T. Loy[d], Kwok-On Lai[a,b,c,2], Amy K. Y. Fu[a,b,c,e], and Nancy Y. Ip[a,b,c,e,3]

[a]Division of Life Science, The Hong Kong University of Science and Technology, Hong Kong, China; [b]Molecular Neuroscience Center, The Hong Kong University of Science and Technology, Hong Kong, China; [c]State Key Laboratory of Molecular Neuroscience, The Hong Kong University of Science and Technology, Hong Kong, China; [d]Department of Physics, The Hong Kong University of Science and Technology, Hong Kong, China; and [e]Guangdong Provincial Key Laboratory of Brain Science, Disease and Drug Development, Hong Kong University of Science and Technology Shenzhen Research Institute, Shenzhen, 518057, China

Contributed by Nancy Y. Ip, July 5, 2017 (sent for review May 18, 2017; reviewed by James Bibb and Lin Mei)

**The experience-dependent modulation of brain circuitry depends on dynamic changes in synaptic connections that are guided by neuronal activity. In particular, postsynaptic maturation requires changes in dendritic spine morphology, the targeting of postsynaptic proteins, and the insertion of synaptic neurotransmitter receptors. Thus, it is critical to understand how neuronal activity controls postsynaptic maturation. Here we report that the scaffold protein liprinα1 and its phosphorylation by cyclin-dependent kinase 5 (Cdk5) are critical for the maturation of excitatory synapses through regulation of the synaptic localization of the major postsynaptic organizer postsynaptic density (PSD)-95. Whereas Cdk5 phosphorylates liprinα1 at Thr701, this phosphorylation decreases in neurons in response to neuronal activity. Blockade of liprinα1 phosphorylation enhances the structural and functional maturation of excitatory synapses. Nanoscale superresolution imaging reveals that inhibition of liprinα1 phosphorylation increases the colocalization of liprinα1 with PSD-95. Furthermore, disruption of liprinα1 phosphorylation by a small interfering peptide, siLIP, promotes the synaptic localization of PSD-95 and enhances synaptic strength in vivo. Our findings collectively demonstrate that the Cdk5-dependent phosphorylation of liprinα1 is important for the postsynaptic organization during activity-dependent synapse development.**

cyclin-dependent kinase 5 | neurodevelopmental disorders | PSD-95 | synaptic plasticity | neuronal activity

The precise formation of neural circuitry is essential for normal brain function and depends on proper synapse development. Dysregulation of synapse development is associated with various neurodevelopmental and psychiatric disorders such as autism, fragile-X syndrome, epilepsy, schizophrenia, and depression (1–3). Synapse development requires the proper localization and recruitment of various components, including glutamate receptors, cytoskeletal elements, and scaffold proteins, to the postsynaptic density (PSD), a process controlled by neuronal activity (4, 5); however, how neuronal activity precisely coordinates the localization of these proteins remains elusive.

Scaffold proteins regulate the structure and functions of synapses through protein–protein interactions and the recruitment of different groups of synaptic proteins (6, 7). In particular, PSD-95, the most abundant scaffold protein in the PSD, interacts with specific synaptic proteins through its multiple protein-interaction domains. It plays essential roles in the organization of the PSD, including stabilizing glutamate receptors at the postsynaptic membrane and organizing adhesion molecules (7). The synaptic localization and clustering of PSD-95 are regulated by neuronal activity (8–10), and loss of PSD-95 perturbs activity-dependent dendritic spine maturation and synaptic strengthening (11). Thus, the precise regulation of PSD-95 localization at synapses is believed to be a key event in the organization and refinement of the postsynaptic apparatus.

The liprinα family comprises abundant scaffold proteins that have been suggested as being critical for synapse organization through their interactions with multiple synaptic proteins (6). At the presynaptic terminals, the interaction of liprinα with the active zone proteins RIM and ELKS/CAST enhances presynaptic assembly and neurotransmitter release (12, 13). At the postsynaptic sites, liprinα regulates the synaptic targeting of AMPA-type glutamate receptors through its interaction with GRIP (6, 14); likewise, it regulates the trafficking of the cadherin–catenin adhesion protein complex through its interaction with the LAR family of receptor protein tyrosine phosphatases (15). Nevertheless, the molecular control that regulates the function of liprinα remains unclear.

Synaptic proteins undergo various posttranslational modifications in response to neuronal activity. One of the primary regulatory events involves protein phosphorylation (16, 17). Cyclin-dependent kinase 5 (Cdk5), a proline-directed serine/threonine kinase, is crucial for the proper development of excitatory synapses (18). Restrained Cdk5 activity promotes synapse maturation and enhances neurotransmission through the suppression of the phosphorylation of its specific substrates during development (19, 20). For example, reduction of the Cdk5-dependent phosphorylation of NMDA receptor subunit NR2B increases NR2B

## Significance

The activity-dependent organization of synaptic components occurs during brain development in response to experience, and involves the precise regulation of the localization of synaptic proteins. However, the molecular mechanisms underlying activity-dependent organization of synaptic proteins remain unclear. We found that inhibition of the phosphorylation of the scaffold protein liprinα1 by neuronal activity promotes the synaptic localization of a major postsynaptic organizer, PSD-95, through increased liprinα1–PSD-95 interaction. This suggests that the phosphorylation status of liprinα1 functions as a molecular control for the activity-dependent localization of PSD-95 and hence postsynaptic organization and synapse maturation. Dysregulation of this posttranslational process may lead to impaired synapse development.

Author contributions: H.H., K.-O.L., A.K.Y.F., and N.Y.I. designed research; H.H., X.L., Z.L., and T.Z. performed research; T.Z., S.D., and M.M.T.L. contributed new reagents/analytic tools; H.H., Z.L., K.-O.L., A.K.Y.F., and N.Y.I. analyzed data; and H.H., A.K.Y.F., and N.Y.I. wrote the paper.

Reviewers: J.B., University of Alabama at Birmingham; and L.M., Medical College of Georgia.

The authors declare no conflict of interest.

Freely available online through the PNAS open access option.

[1]Present address: Division of Chemistry and Chemical Engineering, California Institute of Technology, Pasadena, CA 91125.

[2]Present address: Department of Physiology, The University of Hong Kong, Hong Kong, China.

[3]To whom correspondence should be addressed. Email: boip@ust.hk.

This article contains supporting information online at www.pnas.org/lookup/suppl/doi:10.1073/pnas.1708240114/-/DCSupplemental.

surface expression and thus synaptic transmission (21, 22). Meanwhile, decreased Cdk5-dependent phosphorylation of PSD-95 promotes the synaptic clustering of PSD-95 and its associated glutamate receptors (23). These findings suggest that the precise control of Cdk5-dependent phosphorylation is critical for postsynaptic maturation during synapse development.

In the present study, we report that liprinα1 is phosphorylated by Cdk5, which governs the activity-dependent localization of PSD-95 during synapse development. Specifically, we found that Cdk5 phosphorylates liprinα1 at Thr701 in neurons, and this phosphorylation was reduced in the visual cortex in response to visual stimulation after eye opening. Blockade of liprinα1 phosphorylation in hippocampal neurons promoted excitatory synaptic development, as demonstrated by enhanced dendritic spine maturation and increased surface expression of AMPA-type glutamate receptor subunits. Importantly, increased neuronal activity and inhibition of liprinα1 phosphorylation enhanced the association between liprinα1 and PSD-95, and hence the synaptic localization of PSD-95. Thus, our results demonstrate that the Cdk5-dependent phosphorylation of liprinα1 provides a molecular control during maturation of hippocampal excitatory synapses by regulating the synaptic targeting of PSD-95.

## Results

**Regulation of Cdk5-Dependent Liprinα1 Phosphorylation at Thr701 by Neuronal Activity.** To study the roles of liprinα1 at the hippocampal excitatory synapses, we examined the protein regulation of liprinα1 in the mouse hippocampus during the stage of activity-dependent synapse development and its subcellular distribution at the excitatory synapses. We found that liprinα1 was highly expressed in the mouse hippocampus at postnatal day (P) 7, and decreased gradually thereafter until P30 (Fig. 1*A*). However, examining the expression of liprinα1 in various subcellular fractions of mouse brains revealed that although liprinα1 protein

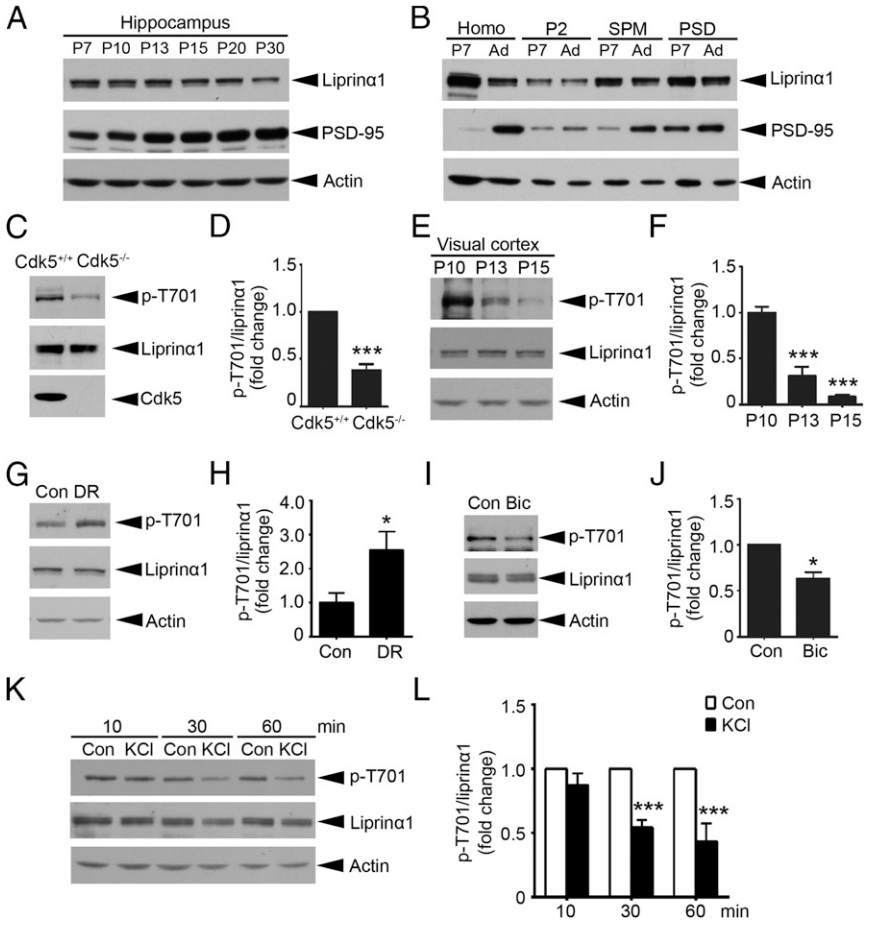


**Fig. 1.** The Cdk5-dependent phosphorylation of liprinα1 is regulated by neuronal activity. (*A*) Developmental profile of liprinα1 in the mouse hippocampus at the indicated stages. The tissue homogenate (P7–P30) were subjected to Western blot analysis for liprinα1, PSD-95, and actin as a loading control (Con). (*B*) Liprinα1 was enriched in the PSD fractions of rat brains at both P7 and the adult stage (Ad). The quality of the SPM and PSD fractions was verified by Western blotting against PSD-95. (*C* and *D*) Liprinα1 phosphorylation (p-T701) was significantly reduced in E18 Cdk5$^{-/-}$ brains compared with Cdk5$^{+/+}$ brains. (*C*) Representative Western blot. (*D*) Quantification analysis of liprinα1 phosphorylation. ***$P < 0.001$, Student's *t* test; $n = 5$ mice per genotype. (*E*–*H*) Liprinα1 phosphorylation in the mouse visual cortex was reduced from P10–P15 but was increased by dark rearing (DR). (*E*) Western blot analysis showing a dramatic reduction of liprinα1 phosphorylation in the mouse visual cortex from P10 to P15. (*F*) Quantification analysis of liprinα1 phosphorylation. ***$P <$ 0.001, one-way ANOVA with the Student–Newman–Keuls test; $n = 3$ mice per condition. (*G* and *H*) DR increased liprinα1 phosphorylation in the mouse visual cortex. (*G*) Western blot analysis. (*H*) Quantification of liprinα1 phosphorylation. *$P < 0.05$, Student's *t* test; $n = 10$ and 11 mice for normal and DR conditions, respectively. (*I* and *J*) Bicuculline (Bic) treatment (40 μM, 24 h) reduced liprinα1 phosphorylation in cultured hippocampal neurons. (*I*) Representative Western blot. (*J*) Quantification analysis of liprinα1 phosphorylation. *$P < 0.05$, Student's *t* test; $n = 3$ independent experiments. (*K* and *L*) KCl treatment (51 mM) reduced liprinα1 phosphorylation in cultured cortical neurons at 17 DIV compared with NaCl (51 mM) as a control (Con). (*K*) For Western blot analysis, neurons were treated with NaCl or KCl for 10, 30, or 60 min. (*L*) Quantification of liprinα1 phosphorylation after KCl treatment or the corresponding NaCl treatment. ***$P < 0.001$, Student's *t* test; $n = 3$ independent experiments. All data are mean ± SEM.

expression was reduced on development, its enrichment in the PSD was greater at the adult stage (Fig. 1*B*). In addition, liprinα1 was distributed as clusters along the dendrites of cultured hippocampal neurons, and these clusters were colocalized with PSD-95 (Fig. S1*A*). These results demonstrate that liprinα1 is enriched in the PSD, suggesting its potential roles in postsynaptic development.

The functions of synaptic proteins can be regulated by rapid and reversible posttranslational modifications, such as phosphorylation (17). We performed a mass spectrometry (MS) study of phosphopeptides generated from Cdk5-conditional knockout mouse brains and wild-type (WT) controls, and identified a phosphopeptide of liprinα that was decreased in Cdk5-conditional knockout mice. Cdk5 generally phosphorylates substrates at the Ser/Thr sites within the consensus motif (S/T)PX(K/H/R) (24). We analyzed the protein sequence of human liprinα1 and found one strong consensus Cdk5 phosphorylation motif, TPRR, located at Thr701, which corresponds to Thr725 in the mouse liprinα1 protein sequence (Fig. S1*B*). To reduce redundancy and avoid confusion, we designated the liprinα1 phosphorylation site as Thr701, which corresponds to Thr725 in mice and Thr700 in rats.

Given the important role of Cdk5 in synapse development (25), we examined whether liprinα1 is a substrate of Cdk5 to provide insight into the regulatory roles of liprinα1 at synapses. In HEK293T cells, human liprinα1 was phosphorylated by Cdk5/p35 at Thr701; meanwhile, mutating this site to alanine (i.e., T701A mutant) completely abolished the phosphorylation (Fig. S1*C*). Pharmacologic inhibition of Cdk5 by roscovitine (Ros) in cultured neurons significantly reduced liprinα1 phosphorylated at Thr701 (Fig. S1 *D* and *E*). Furthermore, we found that liprinα1 phosphorylation was significantly reduced (by ∼62%) in Cdk5-knockout ($Cdk5^{-/-}$) mouse brains compared with the WT controls ($Cdk5^{+/+}$) (Fig. 1 *C* and *D*). Taken together, results demonstrate that Cdk5 is the major kinase that phosphorylates liprinα1 at Thr701 both in vitro and in vivo.

To determine whether Cdk5-dependent phosphorylation regulates the function of liprinα1, we first examined the developmental profile of liprinα1 phosphorylation during brain development. Intriguingly, liprinα1 phosphorylation decreased dramatically in the mouse hippocampus from P10 to P30 (Fig. S1*F*), which encompasses a critical period in synaptogenesis and circuitry formation in the brain (26, 27). The eye-opening process during this period, when visual stimuli accelerate synapse development in the mouse visual cortex, is a widely accepted paradigm for studying activity-dependent synapse development (22, 28); therefore, we determined whether liprinα1 phosphorylation in the mouse visual cortex is regulated by eye opening. To this end, we examined the levels of liprinα1 phosphorylation in the mouse visual cortex before and after eye opening (P10–P15), because mice open their eyes around P12.5 (29). We found that liprinα1 phosphorylation decreased significantly after eye opening (by ∼69% at P13 and ∼91% at P15 vs. P10; Fig. 1 *E* and *F*).

To determine whether the reduction of liprinα1 phosphorylation depends on visual stimulation, we manipulated the neuronal activity of the mice through dark rearing and examined the subsequent changes in liprinα1 phosphorylation in the activity-deprived visual cortex. Interestingly, dark rearing significantly increased liprinα1 phosphorylation in the visual cortex (by ∼155%; Fig. 1 *G* and *H*), indicating that liprinα1 phosphorylation in the mouse visual cortex is tightly controlled by neuronal activity in vivo.

The results of both the eye-opening and dark-rearing experiments suggest that neuronal activity negatively regulates liprinα1 phosphorylation. Corroborating this idea, we found that treatment of cultured neurons with bicuculline, a GABA receptor antagonist that enhances neuronal activity (30), significantly reduced liprinα1 phosphorylation (Fig. 1 *I* and *J*). Neuronal depolarization by KCl treatment also reduced liprinα1 phosphorylation at Thr701 in cortical neurons (Fig. 1 *K* and *L*).

Because stimulation of glutamate receptors is critical for excitatory synaptic transmission, we examined whether glutamate receptor activation also regulates liprinα1 phosphorylation. Accordingly, glutamate treatment also significantly reduced phosphorylated liprinα1 in cultured cortical neurons (Fig. S1 *G* and *H*). Taken together, these findings demonstrate that enhanced neuronal activity reduces liprinα1 phosphorylation at Thr701 in neurons.

**Liprinα1 Phosphorylation Regulates the Structure and Function of Excitatory Synapses.** To explore the role of liprinα1 in synapse development, we designed three specific shRNAs to target endogenous liprinα1: shLIP-1, shLIP-2, and shLIP-3. When transfected into cultured neurons, these shRNAs efficiently knocked down endogenous liprinα1 by ∼70%, ∼50%, and ∼60%, respectively (Fig. S2 *A* and *B*). Liprinα1 knockdown in hippocampal neurons significantly reduced the complexity of dendritic arbors and the density of dendritic protrusions, whereas coexpression of RNAi-resistant human liprinα1 partially rescued these morphological defects (Fig. 2 *A* and *B* and Fig. S2 *C* and *D*). These findings indicate that liprinα1 is required for the development and maintenance of dendrites and dendritic spines.

We next investigated whether liprinα1 is essential for dendritic spine development in vivo. We infected adult mice with lentivirus-based liprinα1 shRNA, which effectively reduced endogenous liprinα1 in the hippocampal CA1 region (shLIP-1; Fig. S2 *E*–*G*). Consistent with our in vitro findings (Fig. 2 *A* and *B*), liprinα1 depletion in CA1 pyramidal neurons led to a significant decrease in the density of dendritic protrusions (Fig. 2 *C* and *D*).

We then examined whether liprinα1 function is regulated by phosphorylation at Thr701. First, we prepared WT liprinα1, its phosphodeficient TA mutant, and its phosphomimetic TE mutant. We confirmed that their expression levels were comparable by immunostaining and Western blot analyses (Fig. S2 *H* and *I*). We subsequently overexpressed WT liprinα1 or its TA or TE mutant in cultured hippocampal neurons at 12 d in vitro (DIV) and examined dendritic spine morphology at 17 DIV (Fig. 2*E*). We found that expression of the TA mutant significantly increased mature spine density, whereas expression of the TE mutant dramatically reduced mature spine density (Fig. 2*F*). In addition, the TA mutant increased the size of dendritic spine heads, whereas the TE mutant decreased spine head size (Fig. 2*G*). In contrast, expression of the WT or phosphomutants did not significantly alter dendritic complexity (Fig. S2 *J* and *K*).

In addition to analyzing the structure of dendritic spines, we investigated whether liprinα1 phosphorylation is involved in the functional changes of synapses. First, we examined whether liprinα1 phosphorylation affects the number of excitatory synapses, as indicated by staining for the postsynaptic marker PSD-95. We analyzed PSD-95 puncta density, which indicates the synaptic localization of PSD-95 and maturation of excitatory synapses (8, 31), in neurons overexpressing different forms of liprinα1 (WT, TA mutant, or TE mutant). We observed that most PSD-95 puncta were at dendritic spines (∼80%) in the control and WT-expressing neurons; meanwhile, TA-overexpressing neurons and TE-overexpressing neurons exhibited significantly increased and decreased PSD-95 puncta density, respectively (mean ± SEM: control, 4.78 ± 0.17/10 μm; WT, 4.75 ± 0.15/10 μm; TA, 5.77 ± 0.22/10 μm; TE, 3.28 ± 0.16/10 μm; Fig. 2 *H* and *I*). Second, because liprinα1 is reported to regulate postsynaptic maturation by facilitating AMPA receptor targeting, specifically the GluA2 subunit (14), we examined whether liprinα1 phosphorylation regulates the surface expression of GluA2, and found that TA overexpression significantly increased the surface level of GluA2, whereas TE overexpression significantly decreased it (Fig. 2 *J* and *K*). Taken together, these results collectively indicate that liprinα1 controls synapse density and maturation, and that its synaptic function is tightly regulated by Cdk5-mediated phosphorylation.

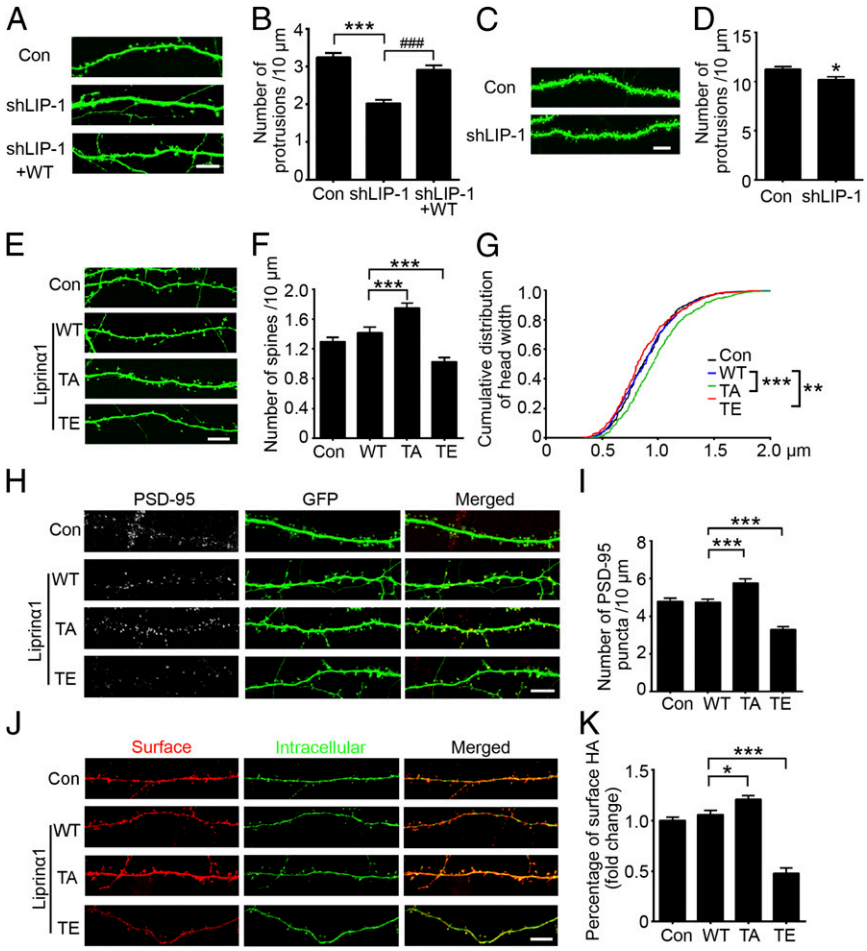


**Fig. 2.** Liprinα1 phosphorylation regulates dendritic spine morphology, PSD-95 localization, and GluA2 surface level. (*A* and *B*) Liprinα1 knockdown significantly reduced the protrusion density of cultured hippocampal neurons, which was partially rescued by RNAi-resistant human liprinα1 (WT). (*A*) Representative images of dendrites from neurons transfected with the indicated plasmids. (Scale bar: 10 μm.) (*B*) Quantification of the dendritic protrusion density of transfected neurons. ***$P < 0.001$ vs. control (Con); $^{###}P < 0.001$ vs. shLIP-1, one-way ANOVA with the Student–Newman–Keuls test. $n = 14$, 12, and 12 neurons for Con, shLIP-1, and shLIP-1+WT, respectively. (*C* and *D*) Liprinα1 knockdown in the mouse hippocampal CA1 region reduced the dendritic protrusion density. (*C*) Representative images of dendrites from virus-infected neurons. (Scale bar: 5 μm.) (*D*) Quantification of the dendritic protrusion density. *$P < 0.05$, Student's *t* test; $n = 24$ and 23 dendrites from three mice each for Con and shLIP-1, respectively. (*E*–*G*) Blockade of liprinα1 phosphorylation by the TA mutant promoted spine maturation, whereas the TE mutant induced the opposite effect. (*E*) Representative dendrite images of neurons transfected with Con, WT, TA, or TE liprinα1. (Scale bar: 10 μm.) (*F*) Quantification of the mature spine density. ***$P < 0.001$ vs. WT, one-way ANOVA with the Student–Newman–Keuls test; $n = 21$, 24, 20, and 24 neurons for Con, WT, TA, and TE, respectively. (*G*) Cumulative distribution curve of spine head width in the Con, WT, TA, and TE overexpression conditions. **$P < 0.01$; ***$P < 0.001$ vs. WT, Kolmogorov–Smirnov test. (*H* and *I*) Overexpression of liprinα1 TA mutant increased PSD-95 puncta density, whereas overexpression of TE mutant decreased PSD-95 puncta density. (*H*) Representative images of PSD-95 puncta distributed along dendrites of neurons transfected with Con, WT, TA, or TE liprinα1. (Scale bar: 10 μm.) (*I*) Quantification of PSD-95 puncta density. ***$P < 0.001$ vs. WT, one-way ANOVA with the Student–Newman–Keuls test; $n = 10$, 11, 9, and 11 neurons for the Con, WT, TA, and TE conditions, respectively. (*J* and *K*) Overexpression of TA liprinα1 mutant increased surface GluA2, whereas overexpression of liprinα1 TE mutant decreased surface GluA2. (*J*) Representative images of surface and intracellular HA staining of transfected neurons. (Scale bar: 10 μm.) (*K*) Quantification analysis of surface GluA2 as indicated by the ratio of HA surface intensity to the total (i.e., surface plus intracellular). *$P < 0.05$; ***$P < 0.001$ vs. WT, one-way ANOVA with the Student–Newman–Keuls test; $n = 22$, 21, 20, and 23 neurons for the Con, WT, TA, and TE conditions, respectively. All data are mean ± SEM.

**Modulation of Liprinα1 Phosphorylation Regulates the Synaptic Localization of PSD-95.** We then examined how suppression of liprinα1 phosphorylation promotes spine maturation and the surface expression of AMPA receptors. Because the precise synaptic localization of PSD-95 is critical for activity-driven synapse maturation (8), we investigated whether liprinα1 phosphorylation specifically regulates PSD-95 localization and function. Given that the functions of liprinα are largely dependent on its interactions with its binding partners (6), we first examined whether liprinα1 interacts with PSD-95. Coimmunoprecipitation revealed an interaction between liprinα1 and PSD-95 in the mouse brain. Notably, the specific interaction of these proteins was significantly enhanced in the mouse brains at ~P13 (Fig. 3 *A* and *B*), the day on which decreased liprinα1 phosphorylation was observed (Fig. 1 *E* and *F*). Therefore, we hypothesized that the inhibition of liprinα1 phosphorylation enhances its interaction with PSD-95.

To determine whether liprinα1 phosphorylation regulates its association with PSD-95 at the synaptic regions, we used the stochastic optical reconstruction microscopy (STORM) superresolution imaging system to examine changes in the subcellular localization of liprinα1 relative to PSD-95 on inhibition of liprinα1 phosphorylation at the nanometer scale. STORM analysis enables the visualization of synaptic proteins in situ, as well as an extremely precise analysis of protein associations and distribution patterns (32, 33). Similar to previous observations, we observed that PSD-95 was expressed as clusters of comparable size, with a mean principal length of 424.7 ± 177.2 nm and an auxiliary length of 282.8 ± 78.85 nm (34).

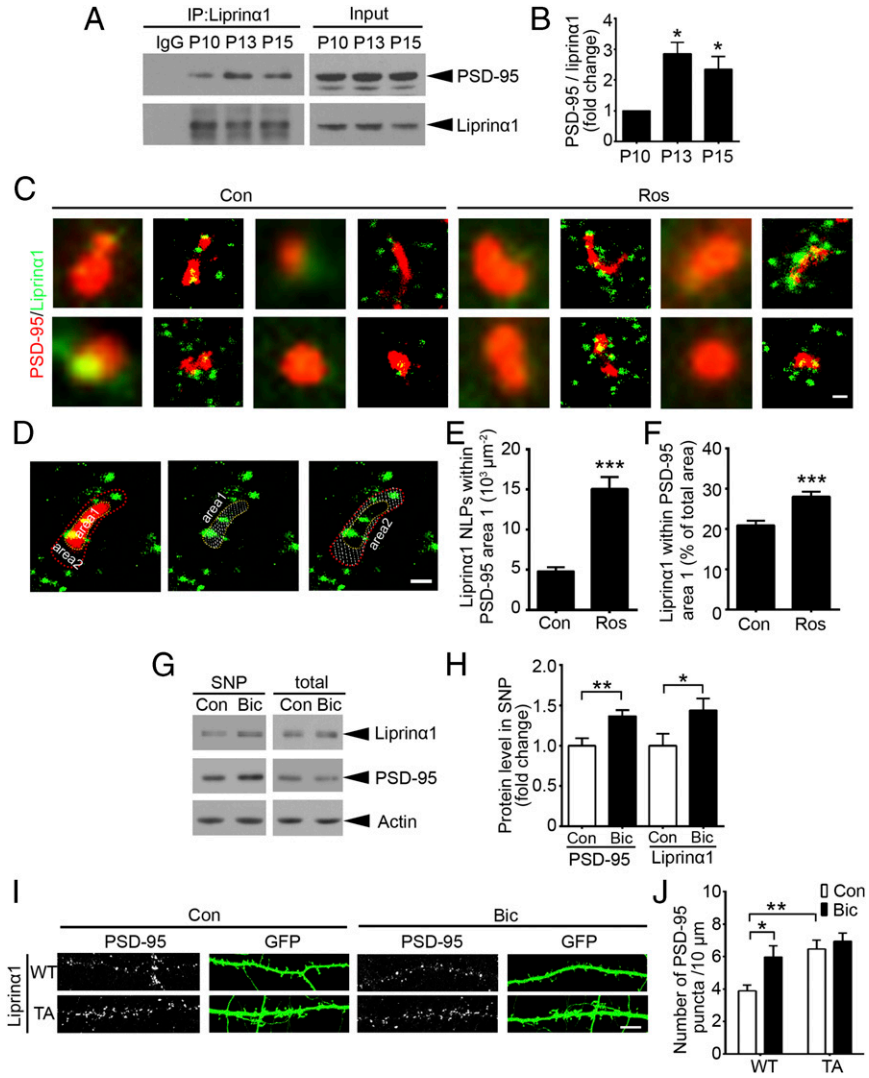


**Fig. 3.** Reduction of liprinα1 phosphorylation enhances liprinα1–PSD-95 binding and promotes PSD-95 synaptic localization. (*A* and *B*) Coimmunoprecipitation of liprinα1 and PSD-95 in mouse brains at P10–P15. (*A*) Representative Western blot. (*B*) Quantification of PSD-95 bound to liprinα1. PSD-95 normalized to immunoprecipitated liprinα1, $*P < 0.05$ vs. P10, one-way ANOVA with the Student–Newman–Keuls test; $n = 3$ independent experiments. (*C*–*F*) Roscovitine (Ros) treatment increased liprinα1 localization density and percentage within the PSD-95 region. Neurons were treated with DMSO as control (Con) or Ros (25 μM) for 2 h and then stained with liprinα1 and PSD-95 after fixation. (*C*) Individual synapses showing the distribution of liprinα1 (green) surrounding PSD-95 (red) in the Con and Ros groups. (Scale bar: 200 nm.) (*D*) Representative images of the defined PSD-95 region (with yellow outline, area 1) and the surrounding region (red outline, area 2); both regions are indicated by dotted slashes. (Scale bar: 200 nm.) (*E* and *F*) Quantification of the localization points (NLPs) of liprinα1 per square micrometer of area 1, and the percentage of liprinα1 within area 1 vs. the total area (area 1 plus area 2). $***P < 0.001$, Student's *t* test; $n = 53$ and 51 synapses for Con and Ros, respectively. (*G* and *H*) Bicuculline (Bic) treatment (40 μM, 24 h) enriched liprinα1 and PSD-95 in the synaptosome, but did not affect their total levels. (*G*) Representative Western blot. (*H*) Quantification of protein level change of liprinα1 and PSD-95 in the synaptosome. $*P < 0.05$; $**P < 0.01$, Student's *t* test; $n = 5$ independent experiments. (*I* and *J*) Bic treatment or overexpression of liprinα1 TA mutant alone increased PSD-95 puncta density. (*I*) Representative images of PSD-95 puncta distributed along the dendrites of neurons overexpressing WT or TA liprinα1 with or without Bic treatment. (Scale bar: 10 μm.) (*J*) Quantification of PSD-95 puncta density. $*P < 0.05$; $**P < 0.01$ vs. WT Con, one-way ANOVA with the Student–Newman–Keuls test; $n = 9$, 12, 8, and 9 neurons for WT Con, WT Bic, TA Con, and TA Bic conditions, respectively. All data are mean ± SEM.

Meanwhile, liprinα1 occurred in clusters smaller than those of PSD-95 (Fig. 3*C* and Fig. S3*A*).

Interestingly, treatment with Ros, which inhibits liprinα1 phosphorylation (Fig. S1 *D* and *E*), increased liprinα1 and PSD-95 colocalization (Fig. 3*C*). Quantitative analysis revealed that Ros treatment significantly increased the localization of liprinα1 within the PSD-95 clusters and induced more liprinα1 recruitment to PSD-95 clusters than to the surrounding regions, as evidenced by the number of localization points and percentage of liprinα1 within the PSD-95 cluster region (Fig. 3 *D*–*F*). Ros treatment also increased the localization of liprinα1 in the region surrounding PSD-95 clusters (Fig. S3*B*). Meanwhile, PSD-95 puncta size was not obviously altered during Ros treatment (Fig. S3*C*), suggesting that the increased colocalization between liprinα1 and PSD-95 is not due to the change in PSD-95 cluster size. Our STORM analysis also suggests that liprinα1 is localized mainly at postsynaptic regions rather than at presynaptic regions, given that liprinα1 was less colocalized with synaptophysin than with PSD-95 (Fig. S3 *D*–*G*). Furthermore, we found that Ros treatment did not alter the colocalization between liprinα1 and synaptophysin (Fig. S3 *H* and *I*). Therefore, our STORM results provide nanoscale-level evidence that the suppression of liprinα1 phosphorylation specifically enhances its association with PSD-95, which may further regulate the synaptic localization of PSD-95 and contribute to postsynaptic development.

To further characterize the role of liprinα1 phosphorylation in the regulation of synaptic localization of PSD-95 on neuronal activity, we treated cultured neurons with bicuculline, which reduces liprinα1 phosphorylation (Fig. 1 *I* and *J*). We detected significant enrichment of PSD-95 together with liprinα1 in the synaptosome (Fig. 3 *G* and *H*), suggesting that the synaptic localization of PSD-95 is enhanced on neuronal activity, which is consistent with previous studies (35). We subsequently examined whether the reduction of liprinα1 phosphorylation is required to mediate the bicuculline-triggered synaptic enrichment of PSD-95. Interestingly, whereas bicuculline treatment enhanced the synaptic enrichment of PSD-95 by increasing PSD-95 puncta density in neurons expressing WT, overexpression of TA mutant alone resulted in the increase of PSD-95 clusters. This finding suggests that decreased liprinα1 phosphorylation mediates the activity-dependent synaptic enrichment of PSD-95 (Fig. 3 *I* and *J*).

**Disruption of Liprinα1 Phosphorylation by Small Interfering Peptide Increases the Synaptic Localization of PSD-95.** To examine the functional roles of endogenous liprinα1 phosphorylation, we

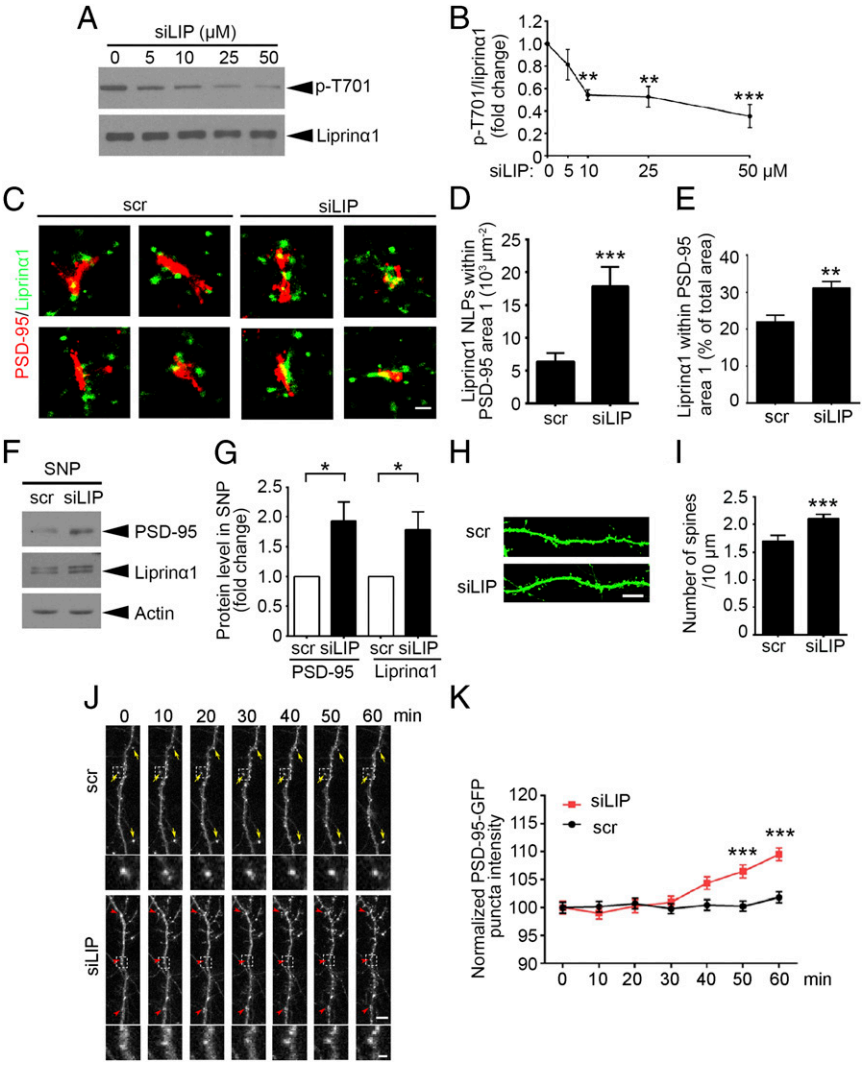


**Fig. 4.** The small phospho-interfering peptide of liprinα1 enhances liprinα1–PSD-95 binding and promotes PSD-95 synaptic localization. (*A* and *B*) The small phospho-interfering peptide of liprinα1 (siLIP) inhibited liprinα1 phosphorylation in a dosage-dependent manner. (*A*) Representative Western blot. Cultured neurons were incubated with siLIP at the indicated dosages for 2 h. (*B*) Quantification of liprinα1 phosphorylation. $^{**}P < 0.01$; $^{***}P < 0.001$, one-way ANOVA with the Student–Newman–Keuls test; $n = 4$ independent experiments. (*C–E*) siLIP treatment (10 μM, 30 min) increased liprinα1 localization density and percentage within the PSD-95 region. (*C*) Individual synapses show the distribution of liprinα1 (green) surrounding PSD-95 (red) in the scramble peptide (scr) and siLIP groups. (Scale bar: 200 nm.) (*D* and *E*) Quantification of the localization points (NLPs) of liprinα1 per square micrometer of area 1, and the percentage of liprinα1 within area 1 vs. the total area (area 1 plus area 2). $^{***}P < 0.001$; $^{**}P < 0.01$, Student's *t* test; $n = 24$ and 20 synapses for scr and siLIP, respectively. (*F* and *G*) siLIP treatment (10 μM, 30 min) enriched liprinα1 and PSD-95 in the synaptosome. (*F*) Representative Western blot. (*G*) Quantification of the protein level changes in liprinα1 and PSD-95 in the synaptosome. $^{*}P < 0.05$, Student's *t* test; $n = 4$ independent experiments. (*H* and *I*) siLIP treatment increased dendritic spine density in cultured hippocampal neurons. (*H*) Representative images of dendrites from neurons treated with scrambled peptide (scr) or siLIP (10 μM, 30 min). (Scale bar: 10 μm.) (*I*) Quantification analysis of the mature spine density. $^{***}P < 0.001$, Student's *t* test; $n = 14$, 16 neurons for the scr and siLIP conditions, respectively. (*J* and *K*) Confocal time-lapse imaging of hippocampal neurons showed that siLIP treatment (10 μM) induced PSD-95 synaptic enrichment. Neurons were transfected with PSD-95–GFP at 14 DIV and imaged at 18–20 DIV. (*J*) Representative images of dendrites showing enriched synaptic localization of PSD-95 after siLIP treatment (*Upper*), and higher-magnification images showing the PSD-95 clusters (*Lower*). Yellow arrow: PSD-95 puncta with similar average intensity; red arrowhead: PSD-95 puncta with increased average intensity. (Scale bar: *Upper*, 5 μm; *Lower*, 1 μm.) (*K*) Quantification of the average intensity of PSD-95–GFP puncta. $^{***}P < 0.001$, two-way ANOVA with Bonferroni post hoc test; $n = 300$~400 puncta for each time point in scr or siLIP treatment. All data are mean ± SEM.

designed a small interfering peptide (siLIP) that specifically targets Cdk5-dependent liprinα1 phosphorylation, corresponding to mouse liprinα1 amino acid residues 718–732 (Fig. S4*A*). We treated cultured neurons with siLIP, which effectively inhibited liprinα1 phosphorylation in vitro in a dose- and time-dependent manner, with an optimal inhibitory effect after 30 min of treatment (Fig. 4 *A* and *B* and Fig. S4 *B* and *C*). We also evaluated the peptide's specificity by examining the phosphorylation of two other well-known Cdk5 substrates, doublecortin (DCX) and WASP-family verprolin homologous protein 1 (WAVE1) (36, 37). The results show that siLIP at a dose ≤10 μM did not affect the phosphorylation of other Cdk5 substrates (Fig. S4 *D* and *E*).

To provide direct evidence that endogenous liprinα1 phosphorylation affects its association with PSD-95, we treated neurons with siLIP and examined the colocalization between liprinα1 and PSD-95 by STORM (Fig. 4*C*). The results provide quantitative evidence that siLIP increases the localization density of liprinα1 and its percentage within PSD-95 clusters (Fig. 4 *D* and *E*). To examine whether the synaptic localization of PSD-95 can be regulated by siLIP, we treated neurons with siLIP and assessed PSD-95 and liprinα1 enrichment in the synaptosomal fraction (Fig. 4 *F* and *G*). Both the density and size of PSD-95 puncta were significantly increased in the neurons treated with siLIP (Fig. S4 *F*–*H*). Specifically, analysis of the dendritic spine morphology revealed an increase in dendritic spine density after siLIP treatment (Fig. 4 *H* and *I*). Notably, time-lapse confocal imaging of PSD-95–GFP-expressing neurons showed that siLIP treatment increased the clustering of PSD-95 in the dendrites, further suggesting that liprinα1 phosphorylation regulates the trafficking of PSD-95 along dendrites (Fig. 4 *J* and *K*). This finding corroborates the idea that inhibition of liprinα1 phosphorylation through the phospho-interfering peptide can increase the synaptic localization of PSD-95.

**Inhibition of Liprinα1 Phosphorylation in Vivo Enhances Synaptic Plasticity.** The foregoing results demonstrated that liprinα1 phosphorylation is inhibited by neuronal activity, and that reduction of liprinα1 phosphorylation promotes the synaptic localization of PSD-95 and synapse maturation in cultured neurons. Therefore, we next explored whether disruption of endogenous liprinα1 phosphorylation by in vivo delivery of siLIP regulates synaptic functions in the brain. We found that injection of siLIP into the mouse hippocampal CA1 region resulted in a significant reduction in liprinα1 phosphorylation levels (Fig. 5 *A* and *B*). Consistent with the foregoing findings, in vivo injection of siLIP significantly increased dendritic spine density in mouse hippocampal CA1 neurons (Fig. 5 *C* and *D*).

Given that changes in dendritic spine density are associated with synaptic plasticity (38, 39), we next asked whether liprinα1 knockdown affects hippocampal long-term potentiation (LTP). Indeed, liprinα1 depletion resulted in an ∼20% reduction in CA3–CA1 LTP induced by theta-burst stimulation (Fig. 5 *E* and *F*), suggesting that liprinα1 is required for normal synaptic plasticity. Furthermore, inhibition of the phosphorylation of liprinα1 by siLIP treatment increased LTP in the hippocampal CA3–CA1 region (Fig. 5 *G* and *H*), suggesting that inhibition of liprinα1 phosphorylation enhances synaptic plasticity. Thus, collectively, our findings suggest that liprinα1 phosphorylation is critical for synapse development and synaptic plasticity.

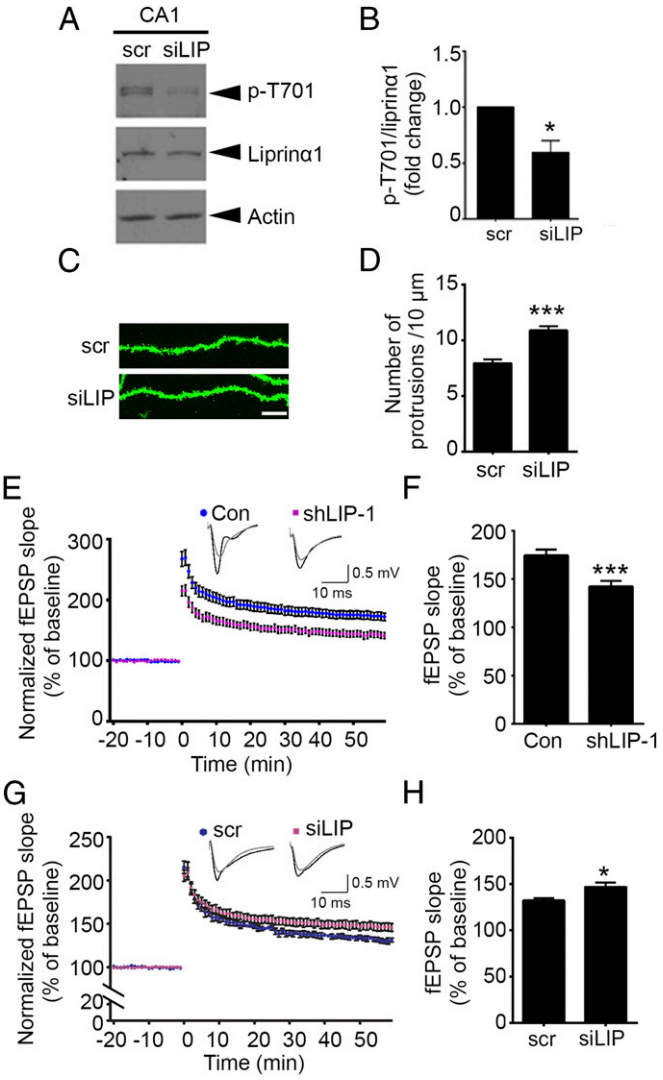


**Fig. 5.** The small phospho-interfering peptide of liprinα1 enhances synaptic plasticity in the hippocampal CA1 region. (*A* and *B*) siLIP injection reduced liprinα1 phosphorylation level in vivo. (*A*) Representative Western blot showing reduced liprinα1 phosphorylation in hippocampal CA1 region at 1 h after siLIP (10 μM) injection. (*B*) Quantification of liprinα1 phosphorylation. $*P <$ 0.05, Student's *t* test; $n = 5$ mice. (*C* and *D*) siLIP injection increased dendritic protrusion density in vivo. (*C*) Representative images of dendrites from hippocampal CA1 neurons. The mouse brains were perfused and fixed at 1 h after scr or siLIP (10 μM) injection. (Scale bar: 10 μm.) (*D*) Quantification of the dendritic protrusion density of infected neurons. $***P < 0.001$, Student's *t* test; $n = 27$ dendrites each from three mice for the scr and siLIP conditions. (*E* and *F*) Liprinα1 knockdown impaired LTP in the mouse hippocampal CA1 region. (*E*) Plots showing normalized field excitatory postsynaptic potential (fEPSP) slope measurement. Sample traces of 5 min before (gray) and 1 h after (black) the theta-burst stimulation are shown. (*F*) Quantification of fEPSP slope at 1 h after LTP induction. $***P < 0.001$, Student's *t* test; $n = 10$ slices from three control (Con) mice and 13 slices from four shLIP-1–infected mice. (*G* and *H*) siLIP peptide enhanced LTP in the mouse hippocampal CA1 region. siLIP (10 μM) was treated 30 min before LTP stimulation. (*G*) Plots of normalized fEPSP slope measurement. Sample traces of 5 min before (gray) and 1 h after (black) the theta-burst stimulation are shown. (*H*) Quantification analysis of fEPSP slope at 1 h after LTP induction. $*P < 0.05$, Student's *t* test; $n = 7$ and 8 slices from a total of six mice for scr and siLIP treatment, respectively. All data are mean ± SEM.

## Discussion

Elucidating the molecular mechanism by which neuronal activity controls synapse development will enhance our understanding of brain functions and help identify potential targets for neurologic disorders. In this study, we found that the activity-dependent down-regulation of liprinα1 phosphorylation governs postsynaptic maturation through the coordinated regulation of the assembly and localization of specific PSD components. In particular, liprinα1 phosphorylation is inhibited during activity-dependent synaptic maturation, which enhances its association with PSD-95 and promotes the synaptic localization and enrichment of PSD-95, and leads to the maturation of dendritic spines and increased surface expression of AMPA-type glutamate receptors. Our findings

reveal that modulation of the phosphorylation status of liprinα1 is essential for neuronal activity-controlled postsynaptic organization during brain development.

As a major component of the PSD, PSD-95 largely determines synapse size and strength through its synaptic localization and clustering (7, 8). On neuronal activity, PSD-95 can be recruited to synaptic regions, as observed in the visual cortex after eye opening, which underlies activity-dependent synapse maturation (29, 40); however, how activity drives the synaptic transport of PSD-95 during development remains elusive. The synaptic localization of PSD-95 can be regulated by its posttranslational modifications, including phosphorylation and palmitoylation, as well as by molecular binding with ephrin-B3 (10, 41–43). In this study, using a small interfering peptide that specifically inhibits liprinα1 phosphorylation, we have shown that inhibition of liprinα1 phosphorylation promotes PSD-95 clustering and its synaptic localization through enhanced interaction between these proteins. On the other hand, motor proteins can complex with liprinα1 (6), and this interaction may be involved in the transport of PSD-95 to synapses. Specifically, KIF1A is a kinesin motor that interacts with liprinα1 and regulates the cargo transport of the liprinα1-associated protein complex (44). Indeed, enrichment of synaptic PSD-95 induced by brain-derived neurotrophic factor is abolished in KIF1A$^{+/-}$ mice (45). Thus, it is of interest to determine whether liprinα1-KIF1A interaction also regulates PSD-95 transport and whether liprinα1 phosphorylation regulates the process.

Given our limited understanding of the domain structure of liprinα1, the structural domains of liprinα1 that mediate the interaction of the protein with its binding partners remain unclear. Liprinα1 is characterized by an N-terminal coiled-coil domain followed by three sterile-α-motif domains and a C-terminal PDZ-binding motif (6). Nonetheless, because the Cdk5-dependent phosphorylation site of liprinα1 is not located at any of the specific domains, how the phosphorylation of liprinα1 specifically affects its association with PSD-95 remains to be determined. In addition, understanding the transport machinery of PSD-95 will provide insight into how the inhibition of liprinα1 phosphorylation facilitates PSD-95 synaptic localization.

Whereas the suppression of Cdk5-dependent liprinα1 phosphorylation promotes the clustering and synaptic localization of PSD-95, Cdk5 inhibits PSD-95 clustering through the direct phosphorylation of various substrates, such as PSD-95 (23) and WAVE1. Specifically, the Cdk5-dependent phosphorylation of WAVE1 inhibits WAVE1 function and negatively regulates actin polymerization and dendritic spine morphology (37). WAVE1 phosphorylation can be partially controlled by cAMP or NMDA receptor-dependent dephosphorylation via PP2A or PP2B (46). Accordingly, it would be of interest to determine whether the activity-dependent decrease of liprinα1 phosphorylation occurs at least in part through phosphatase-mediated dephosphorylation on enhanced neuronal activity (47). Moreover, the phosphorylation status of synaptic substrates also depends on the activity and subcellular localization of kinases (48). Neuronal depolarization stimulates the nuclear transport and enrichment of Cdk5 (49), which may decrease the accessibility of Cdk5 to phosphorylate liprinα1 in dendrites, leading to reduced liprinα1 phosphorylation. Thus, it is critical to determine how neuronal activity regulates Cdk5 activity and its subcellular localization during synapse development.

Based on sequence analysis, the Cdk5-dependent phosphorylation site of liprinα1 (Thr701) is conserved among liprinα family members, including liprinα1, liprinα2, liprinα3, and liprinα4. Although the high homology of the liprinα members may suggest functional redundancy among them, liprinα members have distinct spatiotemporal expression profiles (50). In particular, whereas the protein expression of liprinα1 in the mouse brain decreases during development, the synaptic localization of liprinα1 is enriched in mouse brains at adulthood (Fig. 1*B*). Moreover, protein expression of liprinα1 can be regulated by $Ca^{2+}$/CaMKII (51), suggesting that liprinα1 has specific functions at synapses. These findings collectively suggest that liprinα1 is specifically involved in synapse development.

Although liprinα family members are suggested to regulate presynaptic functions by organizing presynaptic components and mediating neurotransmitter release (6), our STORM results reveal that liprinα1 phosphorylation mainly regulates the localization of liprinα1 within PSD-95 clusters at the postsynaptic region, not presynaptic organization. In addition, we observed a decreased number of dendritic spines in liprinα1-knockdown neurons (Fig. 2), suggesting that liprinα1 has an autonomous role at postsynaptic sites. Taken together, these findings hint at the specific postsynaptic functions of liprinα1. Superresolution light imaging methods have elucidated how PSD-95 and its binding partners organize the nanodomains of AMPA receptors (34, 52). Therefore, it would be of great interest to track the dynamics of liprinα1–PSD-95 interaction together with the organization of AMPA receptors on neuronal activity using superresolution imaging methods. The findings will provide a comprehensive understanding of how liprinα1 phosphorylation regulates postsynaptic functions through protein–protein interactions and PSD organization. Whereas Cdk5 has functional roles at presynaptic regions, including regulating neurotransmitter release (53), it is of interest to determine whether the presynaptic functions of liprinα1 are regulated by its Cdk5-dependent phosphorylation.

In conclusion, the present study demonstrates that the activity-dependent regulation of Cdk5-dependent liprinα1 phosphorylation promotes the synaptic localization of PSD-95 and hence postsynaptic maturation. Our findings provide insight into the mechanisms underlying postsynaptic organization and sensory-driven synapse development. Dysregulation of the abovementioned process may lead to the malformation of excitatory synapses, a process that underlies various neurodevelopmental disorders. Thus, identifying how the postsynaptic assembly is regulated in a phosphorylation-dependent manner and delineating the regulation of protein–protein interactions at the postsynaptic regions at the nanoscale level may help elucidate the mechanisms that underlie synaptic dysfunctions in neurodevelopmental disorders.

## Materials and Methods

**Antibodies and Constructs.** The antibody against the phosphorylated liprinα1 at Thr701 (p-T701) was raised by immunizing a rabbit with a synthetic phospho-peptide containing the phospho-Thr725 residue of mouse liprinα1 [GRST(P)PRRVPHSPARC, amino acids 722–735; Bio-Synthesis]. Serum from the immunized rabbit was purified twice sequentially using two Sulfolink columns (Pierce Biotechnology) containing beads coupled with a nonphosphorylated peptide (GRSTPRRVPHSPARC; Bio-Synthesis). The elution of the first column yielded the total liprinα1 antibody. The phospho-specific liprinα1 antibody was subsequently purified by eluting the third Sulfolink column conjugated with the phospho-peptide. The other antibodies and chemicals used in this study are described in *SI Materials and Methods*.

The following expression constructs were used in the study: N-terminal FLAG-tagged full-length human liprinα1 in pcDNA 3.0 vector subcloned from human liprinα1 (Invitrogen) and its point mutants at Thr701 (TA and TE); constructs encoding human Cdk5 and mouse p35 (30); HA-tagged full-length GluA2 [provided by Jun Xia, The Hong Kong University of Science and Technology (HKUST)]; and pSUPER-based shRNA constructs targeting mouse and rat liprinα1 sequences (shLIP-1: 5′-GTCTGAAGAGATGAATACG-3′; shLIP-2: 5′-GTTGCATGAAGTTGGTCAT-3′; shLIP-3: 5′-GTTGCTCTCAGAATCCAAT-3′).

The scrambled and phospho-interfering peptides were purchased from Bio-Synthesis and were verified by MS analysis and reverse-phase HPLC. The sequences of the small interfering peptide of liprinα1 and scrambled control peptide (scr) were PPGSGRSTPRRVPHS and SGPSRPTPHSGRPVR, respectively. The cell-penetrating sequence (RQIKIWFQNRRMKWKK) was attached to the N terminus of the peptide as described previously (21).

**Neuronal Cultures and Transfection.** For primary neuronal cultures, cortical and hippocampal neurons were collected from rat brains at embryonic day (E) 18, seeded onto Petri dishes coated with poly-D-lysine (Sigma-Aldrich), and

cultured in Neurobasal medium (Invitrogen) containing 2% (vol/vol) B27 (Invitrogen) at 37 °C in 5% $CO_2$. The hippocampal neurons were transfected at 12 or 16 DIV with the indicated plasmids (30).

**Animals and Dark Rearing.** C57 mice of the indicated ages were obtained from the HKUST Animal Care Facility, and the Cdk5-knockout mice were obtained as described previously (30). For the dark-rearing experiment, the littermates were divided at random into two equal groups after birth: one group reared under normal conditions (12/12-h light/dark) and the other group reared in the dark in ventilated and completely light-proof shells from P2–P14. The visual cortices from both groups were collected for Western blot analysis as described previously (29). All animal procedures were conducted in accordance with the guidelines of the HKUST Animal Care Facility and were approved by the HKUST Animal Ethics Committee.

**In Vitro Phosphorylation Assay.** The in vitro phosphorylation assay was performed as described previously (30). In brief, the indicated constructs were overexpressed in the HEK293T cells. Then the FLAG-tagged wild-type (WT) or the TA mutant of liprinα1 was immunoprecipitated from HEK293T cell lysates using anti-FLAG M2 agarose beads (Sigma-Aldrich) and eluted with sample buffer after 2 h of pull-down at 4 °C. The samples were resolved by SDS/PAGE, followed by Western blot analysis with specific antibodies.

**Immunocytochemistry.** For the costaining of total liprinα1 and PSD-95, the low-density hippocampal neurons were fixed at 23 DIV with methanol at −20 °C for 15 min. The neurons were subsequently incubated with primary antibodies against liprinα1 (1:250) and PSD-95 (1:500) diluted in GDB buffer (30 mM phosphate buffer [pH 7.4] containing 0.2% gelatin by weight, 0.5% Triton X-100, and 0.8 M NaCl) overnight at 4 °C. After three washes with washing buffer (20 mM phosphate buffer and 0.5 M NaCl), the neurons were incubated with Alexa Fluor-conjugated secondary antibodies (diluted in GDB buffer) at 22–25 °C for 1 h, washed three times in washing buffer, and then mounted in Hydromount (National Diagnostics). The sequential staining of surface and intracellular HA was performed as described previously (54). For the GFP staining of virus-infected mouse hippocampi, the brains were fixed with 4% paraformaldehyde. Then, 40-μm of brain sections were collected using a vibrating tissue slicer (VT 1000S; Leica) and were incubated with GFP antibody overnight followed by DAPI for 1 h.

**Image Acquisition and Quantification.** For confocal imaging, the liprinα1 and PSD-95 costaining was imaged using an Olympus Fluoview FV1000 confocal microscope with a 60× oil-immersion objective. Between 8 and 12 serial optical sections (Z-interval, 0.5 μm) were collected. Images of dendritic spines in virus-injected mouse hippocampal CA1 regions were acquired with a Leica SP8 confocal microscope with a 63× oil-immersion objective in the Z-serial scanning mode. Meanwhile, the images of dendritic spines in GFP-transfected hippocampal neurons were acquired with a Nikon A1 confocal microscope with a 60× oil-immersion objective. All images were analyzed using Metamorph version 7.7. Details of the analysis of dendrite and dendritic spine morphology, as well as the surface expression level of HA-GluA2, are provided in *SI Materials and Methods*.

The superresolution images were acquired with a custom-built STORM system designed specifically for the dual-channel imaging of Alexa Fluor 647- and Alexa Fluor 750-immunolabeled samples as described previously (55). Each superresolution image was reconstructed from a 30,000-frame movie of blinking molecules. Moderate excitation laser intensities (4 kW/cm$^2$ at 656 nm for Alexa Fluor 647; 4.5 kW/cm$^2$ at 750 nm for Alexa Fluor 750) were applied to minimize photobleaching during imaging. The final resolution was <20 nm in both channels, determined based on the average fitting error. Details of the quantification of the localization of liprinα1 with respect to PSD-95 or synaptophysin in individual synapses are provided in *SI Materials and Methods*.

**Stereotaxic Surgery and Electrophysiology.** Virus delivery was performed as described previously (56). Liprinα1 was knocked down in the mouse hippocampus by delivering VSV-G pseudotyped lentivirus particles with pFUGW-shLIP-1 (vector served as a control) into the hippocampal CA1 region (anteroposterior, −2.00 mm; mediolateral, ±1.7 mm; dorsoventral, −1.5 mm; all coordinates relative to bregma) for 4 wk (19). The lentivirus was injected at 0.1 μL min$^{-1}$ using a Quintessential Stereotaxic Injector (53311; Stoelting), with injection volumes of 1 μL for the spine morphology study and 3 μL for the LTP analysis. For in vivo peptide delivery, scr or siLIP (10 μM) was mixed with Evans blue dye before being injected into either side of the hippocampal CA1 region in adult mice (age 2–3 mo). At 1 h after injection, the mouse brains were dissected, and the dye-infected areas of the CA1 region were subsequently obtained for protein analysis.

LTP was measured as described previously (56). In brief, acute mouse hippocampal slices (300 μm) were collected using a vibrating tissue slicer (HM650V; Thermo Fisher Scientific) and were recovered in 95%$O_2$/5%$CO_2$ oxygenated artificial cerebrospinal fluid at 32 °C for 2 h. The field excitatory postsynaptic potential (fEPSP) was recorded using a MED64 multichannel recording system (Alpha MED Scientific). The LTP in each slice was induced with one train of theta-burst stimulation consisting of ten 5-Hz series of four 100-Hz pulses. The fEPSP slope from 20 min before to 60 min after the stimulus was analyzed.

**Statistical Analysis.** All data are expressed as mean ± SEM. The unpaired Student's *t* test (two-sided) or one-way ANOVA was used followed by the Student–Newman–Keuls post hoc test to evaluate the significance of differences between two experimental conditions and three or more experimental conditions, respectively. All of the experiments were performed at least in triplicate unless indicated otherwise. The level of significance was set at $P < 0.05$.

Detailed descriptions of the generation of site mutants, cell culture, transfection, immunoprecipitation, and Western blot analysis are provided in *SI Materials and Methods*.

**ACKNOWLEDGMENTS.** We thank Dr. Jun Xia (The Hong Kong University of Science and Technology) for the HA-tagged GluA2 plasmid; Dr. Paul Greengard (Rockefeller University) for the phospho-WAVE1 antibody; Cara Kwong, Busma Butt, Nelson Hung, and Dr. Edward Tam for their excellent technical assistance; Dr. Yang Shen for professional suggestions about electrophysiology experiments; and other members of the N.Y.I. laboratory for their helpful discussions. This study was supported in part by the Research Grants Council of Hong Kong Special Administrative Region (Grants HKUST 660213, HKUST 661013, HKUST 16124616, and HKUST12/CRF/13G), the National Key Basic Research Program of China (Grant 2013CB530900), the Hong Kong Research Grants Council Theme-Based Research Scheme (Grant T13-607/12R), the Area of Excellence Scheme of the University Grants Committee (Grant AoE/M-604/16), and the Shenzhen Peacock Plan.

1. Gai X, et al. (2012) Rare structural variation of synapse and neurotransmission genes in autism. *Mol Psychiatry* 17:402–411.
2. Pfeiffer BE, et al. (2010) Fragile X mental retardation protein is required for synapse elimination by the activity-dependent transcription factor MEF2. *Neuron* 66:191–197.
3. Waites CL, Garner CC (2011) Presynaptic function in health and disease. *Trends Neurosci* 34:326–337.
4. Garner CC, Zhai RG, Gundelfinger ED, Ziv NE (2002) Molecular mechanisms of CNS synaptogenesis. *Trends Neurosci* 25:243–251.
5. Hua JY, Smith SJ (2004) Neural activity and the dynamics of central nervous system development. *Nat Neurosci* 7:327–332.
6. Spangler SA, Hoogenraad CC (2007) Liprin-alpha proteins: Scaffold molecules for synapse maturation. *Biochem Soc Trans* 35:1278–1282.
7. Kim E, Sheng M (2004) PDZ domain proteins of synapses. *Nat Rev Neurosci* 5:771–781.
8. El-Husseini AE-D, Schnell E, Chetkovich DM, Nicoll RA, Bredt DS (2000) PSD-95 involvement in maturation of excitatory synapses. *Science* 290:1364–1368.
9. Schnell E, et al. (2002) Direct interactions between PSD-95 and stargazin control synaptic AMPA receptor number. *Proc Natl Acad Sci USA* 99:13902–13907.
10. El-Husseini Ael-D, et al. (2002) Synaptic strength regulated by palmitate cycling on PSD-95. *Cell* 108:849–863.
11. Ehrlich I, Klein M, Rumpel S, Malinow R (2007) PSD-95 is required for activity-driven synapse stabilization. *Proc Natl Acad Sci USA* 104:4176–4181.
12. Schoch S, et al. (2002) RIM1alpha forms a protein scaffold for regulating neurotransmitter release at the active zone. *Nature* 415:321–326.
13. Ko J, Na M, Kim S, Lee J-R, Kim E (2003) Interaction of the ERC family of RIM-binding proteins with the liprin-α family of multidomain proteins. *J Biol Chem* 278:42377–42385.
14. Wyszynski M, et al. (2002) Interaction between GRIP and liprin-α/SYD2 is required for AMPA receptor targeting. *Neuron* 34:39–52.
15. Dunah AW, et al. (2005) LAR receptor protein tyrosine phosphatases in the development and maintenance of excitatory synapses. *Nat Neurosci* 8:458–467.
16. Chen C-K, et al. (2014) Activity-dependent facilitation of Synaptojanin and synaptic vesicle recycling by the Minibrain kinase. *Nat Commun* 5:4246.
17. Tweedie-Cullen RY, Reck JM, Mansuy IM (2009) Comprehensive mapping of post-translational modifications on synaptic, nuclear, and histone proteins in the adult mouse brain. *J Proteome Res* 8:4966–4982.
18. Su SC, Tsai LH (2011) Cyclin-dependent kinases in brain development and disease. *Annu Rev Cell Dev Biol* 27:465–491.
19. Zhang P, Fu W-Y, Fu AKY, Ip NY (2015) S-nitrosylation-dependent proteasomal degradation restrains Cdk5 activity to regulate hippocampal synaptic strength. *Nat Commun* 6:8665.
20. Zhang S, Edelmann L, Liu J, Crandall JE, Morabito MA (2008) Cdk5 regulates the phosphorylation of tyrosine 1472 NR2B and the surface expression of NMDA receptors. *J Neurosci* 28:415–424.

21. Plattner F, et al. (2014) Memory enhancement by targeting Cdk5 regulation of NR2B. *Neuron* 81:1070–1083.
22. Katz LC, Shatz CJ (1996) Synaptic activity and the construction of cortical circuits. *Science* 274:1133–1138.
23. Morabito MA, Sheng M, Tsai LH (2004) Cyclin-dependent kinase 5 phosphorylates the N-terminal domain of the postsynaptic density protein PSD-95 in neurons. *J Neurosci* 24:865–876.
24. Dhavan R, Tsai L-H (2001) A decade of CDK5. *Nat Rev Mol Cell Biol* 2:749–759.
25. Cheung ZH, Ip NY (2007) The roles of cyclin-dependent kinase 5 in dendrite and synapse development. *Biotechnol J* 2:949–957.
26. Micheva KD, Beaulieu C (1996) Quantitative aspects of synaptogenesis in the rat barrel field cortex with special reference to GABA circuitry. *J Comp Neurol* 373: 340–354.
27. Zheng J-J, et al. (2014) Oxytocin mediates early experience-dependent cross-modal plasticity in the sensory cortices. *Nat Neurosci* 17:391–399.
28. Tian N, Copenhagen DR (2001) Visual deprivation alters development of synaptic function in inner retina after eye opening. *Neuron* 32:439–449.
29. Yoshii A, et al. (2011) TrkB and protein kinase Mζ regulate synaptic localization of PSD-95 in developing cortex. *J Neurosci* 31:11894–11904.
30. Fu W-Y, et al. (2007) Cdk5 regulates EphA4-mediated dendritic spine retraction through an ephexin1-dependent mechanism. *Nat Neurosci* 10:67–76.
31. Parsons MP, et al. (2014) Bidirectional control of postsynaptic density-95 (PSD-95) clustering by Huntingtin. *J Biol Chem* 289:3518–3528.
32. Dani A, Huang B, Bergan J, Dulac C, Zhuang X (2010) Superresolution imaging of chemical synapses in the brain. *Neuron* 68:843–856.
33. Dudok B, et al. (2015) Cell-specific STORM super-resolution imaging reveals nanoscale organization of cannabinoid signaling. *Nat Neurosci* 18:75–86.
34. Nair D, et al. (2013) Super-resolution imaging reveals that AMPA receptors inside synapses are dynamically organized in nanodomains regulated by PSD95. *J Neurosci* 33:13204–13224.
35. Ehlers MD (2003) Activity level controls postsynaptic composition and signaling via the ubiquitin-proteasome system. *Nat Neurosci* 6:231–242.
36. Tanaka T, et al. (2004) Cdk5 phosphorylation of doublecortin ser297 regulates its effect on neuronal migration. *Neuron* 41:215–227.
37. Kim Y, et al. (2006) Phosphorylation of WAVE1 regulates actin polymerization and dendritic spine morphology. *Nature* 442:814–817.
38. Engert F, Bonhoeffer T (1999) Dendritic spine changes associated with hippocampal long-term synaptic plasticity. *Nature* 399:66–70.
39. Lai K-O, Ip NY (2013) Structural plasticity of dendritic spines: The underlying mechanisms and its dysregulation in brain disorders. *Biochim Biophys Acta* 1832:2257–2263.
40. Yoshii A, Sheng MH, Constantine-Paton M (2003) Eye opening induces a rapid dendritic localization of PSD-95 in central visual neurons. *Proc Natl Acad Sci USA* 100: 1334–1339.
41. Craven SE, El-Husseini AE, Bredt DS (1999) Synaptic targeting of the postsynaptic density protein PSD-95 mediated by lipid and protein motifs. *Neuron* 22:497–509.
42. Kim MJ, et al. (2007) Synaptic accumulation of PSD-95 and synaptic function regulated by phosphorylation of serine-295 of PSD-95. *Neuron* 56:488–502.
43. Hruska M, Henderson NT, Xia NL, Le Marchand SJ, Dalva MB (2015) Anchoring and synaptic stability of PSD-95 is driven by ephrin-B3. *Nat Neurosci* 18:1594–1605.
44. Shin H, et al. (2003) Association of the kinesin motor KIF1A with the multimodular protein liprin-alpha. *J Biol Chem* 278:11393–11401.
45. Kondo M, Takei Y, Hirokawa N (2012) Motor protein KIF1A is essential for hippocampal synaptogenesis and learning enhancement in an enriched environment. *Neuron* 73:743–757.
46. Ceglia I, Kim Y, Nairn AC, Greengard P (2010) Signaling pathways controlling the phosphorylation state of WAVE1, a regulator of actin polymerization. *J Neurochem* 114:182–190.
47. Winder DG, Sweatt JD (2001) Roles of serine/threonine phosphatases in hippocampal synaptic plasticity. *Nat Rev Neurosci* 2:461–474.
48. Smith DS, Tsai L-H (2002) Cdk5 behind the wheel: A role in trafficking and transport? *Trends Cell Biol* 12:28–36.
49. Liang Z, et al. (2015) Cdk5 regulates activity-dependent gene expression and dendrite development. *J Neurosci* 35:15127–15134.
50. Zürner M, Mittelstaedt T, tom Dieck S, Becker A, Schoch S (2011) Analyses of the spatiotemporal expression and subcellular localization of liprin-α proteins. *J Comp Neurol* 519:3019–3039.
51. Hoogenraad CC, et al. (2007) Liprinalpha1 degradation by calcium/calmodulin-dependent protein kinase II regulates LAR receptor tyrosine phosphatase distribution and dendrite development. *Dev Cell* 12:587–602.
52. Barrera-Ocampo A, Chater TE (2013) Contribution of postsynaptic molecules to AMPA receptor nanodomain organization. *J Neurosci* 33:19048–19050.
53. Kim SH, Ryan TA (2010) CDK5 serves as a major control point in neurotransmitter release. *Neuron* 67:797–809.
54. Lee SH, Simonetta A, Sheng M (2004) Subunit rules governing the sorting of internalized AMPA receptors in hippocampal neurons. *Neuron* 43:221–236.
55. Zhao T, et al. (2015) A user-friendly two-color super-resolution localization microscope. *Opt Express* 23:1879–1887.
56. Shen Y, Fu WY, Cheng EY, Fu AK, Ip NY (2013) Melanocortin-4 receptor regulates hippocampal synaptic plasticity through a protein kinase A-dependent mechanism. *J Neurosci* 33:464–472.
57. Fang WQ, et al. (2011) Cdk5-mediated phosphorylation of Axin directs axon formation during cerebral cortex development. *J Neurosci* 31:13613–13624.
58. Ye T, Ip JPK, Fu AKY, Ip NY (2014) Cdk5-mediated phosphorylation of RapGEF2 controls neuronal migration in the developing cerebral cortex. *Nat Commun* 5:4826.
59. Fu AK, et al. (2014) Blockade of EphA4 signaling ameliorates hippocampal synaptic dysfunctions in mouse models of Alzheimer's disease. *Proc Natl Acad Sci USA* 111: 9959–9964.
60. Lai K-O, et al. (2012) TrkB phosphorylation by Cdk5 is required for activity-dependent structural plasticity and spatial memory. *Nat Neurosci* 15:1506–1515.

# Supporting Information

## Huang et al. 10.1073/pnas.1708240114

### SI Materials and Methods

**Antibodies and Chemicals.** The following antibodies were used at the indicated dilutions: mouse anti–PSD-95 (1:500–1:2,000, MA1-046; Thermo Fisher Scientific), mouse anti-synaptophysin (1:3,000, MAB5258, EMD Millipore), mouse anti-GluA2 (1:1,000, MAB397; EMD Millipore), mouse anti-FLAG (1:5,000, F1804; Sigma-Aldrich), anti–β-actin (1:5,000, A3853; Sigma-Aldrich), mouse anti-Cdk5 (1:5,000, DC-17; Santa Cruz Biotechnology), mouse anti-Arc (1:500, C-7; Santa Cruz Biotechnology), rabbit anti-HA (1:2,000, Y-11; Santa Cruz Biotechnology), mouse anti-HA (1:1,000, 326700; Invitrogen), mouse anti-GFP (1:1,000, A-11120; Invitrogen), rabbit anti–phospho-DCX (p-DCX, Ser297, 1:1,000, 4605; Cell Signaling Technology), and rabbit anti-p35 (1:1,000, C64B10; Cell Signaling Technology). The antibody against phospho-WAVE1 (Ser310, 1:2,000) was a gift from P. Greengard, The Rockefeller University.

The chemicals used in this study included roscovitine (Ros; Calbiochem), bicuculline (bic; Sigma-Aldrich), KCl (Sigma-Aldrich), NaCl (USB; GE Healthcare), and glutamate (Sigma-Aldrich). All chemicals were of analytical grade and used as received without any further purification.

**Site-Directed Mutagenesis.** The site-directed mutagenesis of liprinα1 was performed with oligonucleotide primers designed to substitute the threonine residue with alanine (TA) or glutamic acid (TE) using the QuikChange Site-Directed Mutagenesis Kit (Stratagene) as described previously (57).

**Cell Cultures, Transfection, and Protein Extraction.** HEK293T cells were transfected using Lipofectamine with Plus Reagent (Invitrogen) according to the manufacturer's instructions. The cells were harvested at 24 h after transfection for protein extraction, Western blot analysis, and coimmunoprecipitation analysis. The knockdown efficiencies of liprinα1 shRNAs were evaluated in cultured neurons as described previously (58). The cortical or hippocampal neurons at 14–16 DIV were subjected to various chemical treatments. The neurons were lysed in RIPA buffer containing protease and phosphatase inhibitors as described previously (30).

**Immunoprecipitation and Western Blot Analysis.** The synaptosome and PSD fractions were prepared as described previously (30, 59, 60). In brief, the brain homogenate was centrifuged at 1,000 × *g* at 4 °C for 5 min, and the supernatant was centrifuged at 10,000 × *g* at 4 °C for 15 min to yield the synaptosomal fraction. Following suspension in 4 mM Hepes buffer, the supernatant was centrifuged at 25,000 × *g* for 20 min. The pellet was resuspended in a sucrose discontinuous gradient and centrifuged at 150,000 × *g* for 2 h. The membrane floating between the sucrose gradient was harvested, diluted in Hepes buffer, and centrifuged at 150,000 × *g* for another 30 min to generate the SPM fraction. The SPM was resuspended in Hepes buffer and lysed with 0.5% Triton X-100 for 15 min, after which the mixture was centrifuged at 32,000 × *g* for 20 min to generate the PSD pellet. For coimmunoprecipitation, the neurons were lysed in buffer A (20 mM Tris pH 7.6, 50 mM NaCl, 1 mM EDTA, 1 mM NaF, and 0.5% Nonidet P-40) with protease and phosphatase inhibitors. The mouse brains were homogenized in PBS plus protease and phosphatase inhibitors. The protein lysate was incubated with the corresponding antibody (1:1,000) overnight at 4 °C and subsequently with 50 μL protein G-Sepharose for 1 h at 4 °C. The samples were washed with buffer A and resolved in SDS sample buffer. The coimmunoprecipitated proteins were examined by Western blot analysis as described previously (30).

**Image Analysis and Quantification.** To analyze spine morphology, we analyzed the following parameters of three representative dendrite segments from each neuron: spine head width, neck width, and spine length. We defined the protrusions with a head width/neck width ratio >1.5 as mature dendritic spines. Three dendrites were selected for each neuron, and the dendrite morphology was analyzed in two ways: by quantifying the number of dendrites using ImageJ software with the NeuronJ plugin and by measuring the number of dendritic intersections by Sholl analysis with the Sholl analysis plugin as described previously (19, 49). The ratio of surface HA signal was quantified as described previously (54). In brief, after setting the threshold with respect to the background of all images in each experiment, the total intensities of the surface and intracellular HA signals were quantified; the ratio of the surface HA signal was obtained by dividing the intensity of the surface HA signal by the total HA signal.

To measure and quantify the changes in liprinα1 distribution with respect to PSD-95 or synaptophysin in synapses of STORM images, 1.2 × 1.2-μm (i.e., 400 × 400-pixel) synaptic regions centered on PSD-95 were cropped out. In each cropped image, the outline of PSD-95 was determined by thresholding the grayscale STORM image, designating it "area 1." "Area 2" was defined as the region that doubles each dimension of area 1 but excludes area 1 to represent the peripheral area of PSD-95. The information regarding the relative distribution of liprinα1 within these two regions was obtained by summing the localization counts of liprinα1 within area 1 or area 2. The density of liprinα1 localization was obtained by further dividing the total number of localizations by the corresponding area. Quantitative analysis was performed by constructing the outline of PSD-95 and measuring the localization points of liprinα1 in the indicated areas.

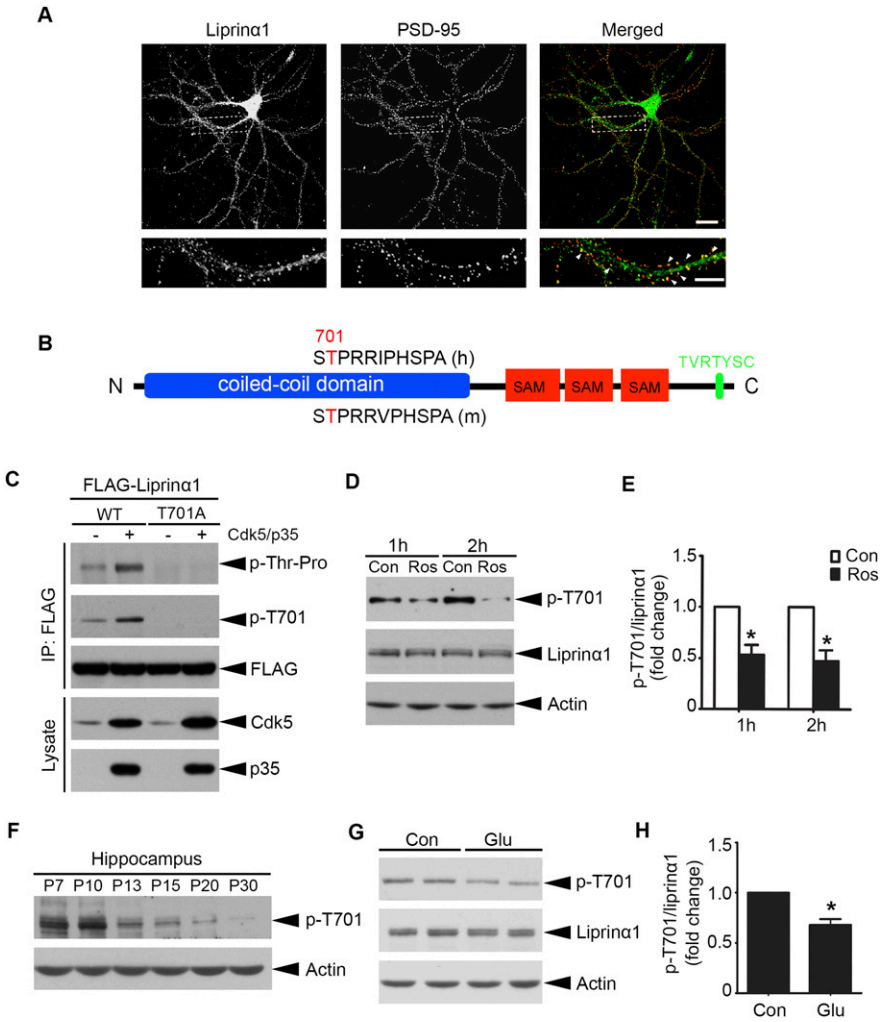


**Fig. S1.** Cdk5-dependent phosphorylation of liprinα1 is regulated by neuronal activity. (*A*) Representative images of cultured hippocampal neurons costained with liprinα1 (green) and PSD-95 (red) at 23 DIV. (Scale bar: *Upper*, 25 μm; *Lower*, 10 μm.) (*B*) Schematic of liprinα1 indicating domains and motifs. The conserved TP (proline-directed threonine) sites of liprinα1 in human (h) and mouse (m) are highlighted in red (positions 701 and 725, respectively). The C-terminal PDZ-binding motif is highlighted in green. (*C*) Phosphorylation of liprinα1 by Cdk5 in HEK293T cells. WT liprinα1 or TA mutant was transfected with or without Cdk5/p35. (*D* and *E*) Roscovitine (Ros; 25 μM) treatment for 1 or 2 h reduced liprinα1 phosphorylation in cultured cortical neurons at 14–16 DIV. (*D*) Representative Western blot. (*E*) Quantification analysis of liprinα1 phosphorylation $^*P < 0.05$, Student's *t* test; $n = 3$ independent experiments. Data are mean ± SEM. (*F*) Developmental profile of liprinα1 phosphorylation (p-T701) in the mouse hippocampus at the indicated stages, with actin serving as a loading control. (*G* and *H*) Glutamate (Glu) treatment (50 μM, 10 min) reduced liprinα1 phosphorylation level in cultured cortical neurons at 14–16 DIV. (*G*) Representative Western blot. (*H*) Quantification analysis of liprinα1 phosphorylation. $^*P < 0.05$, Student's *t* test; $n = 4$ independent experiments. Data are mean ± SEM.

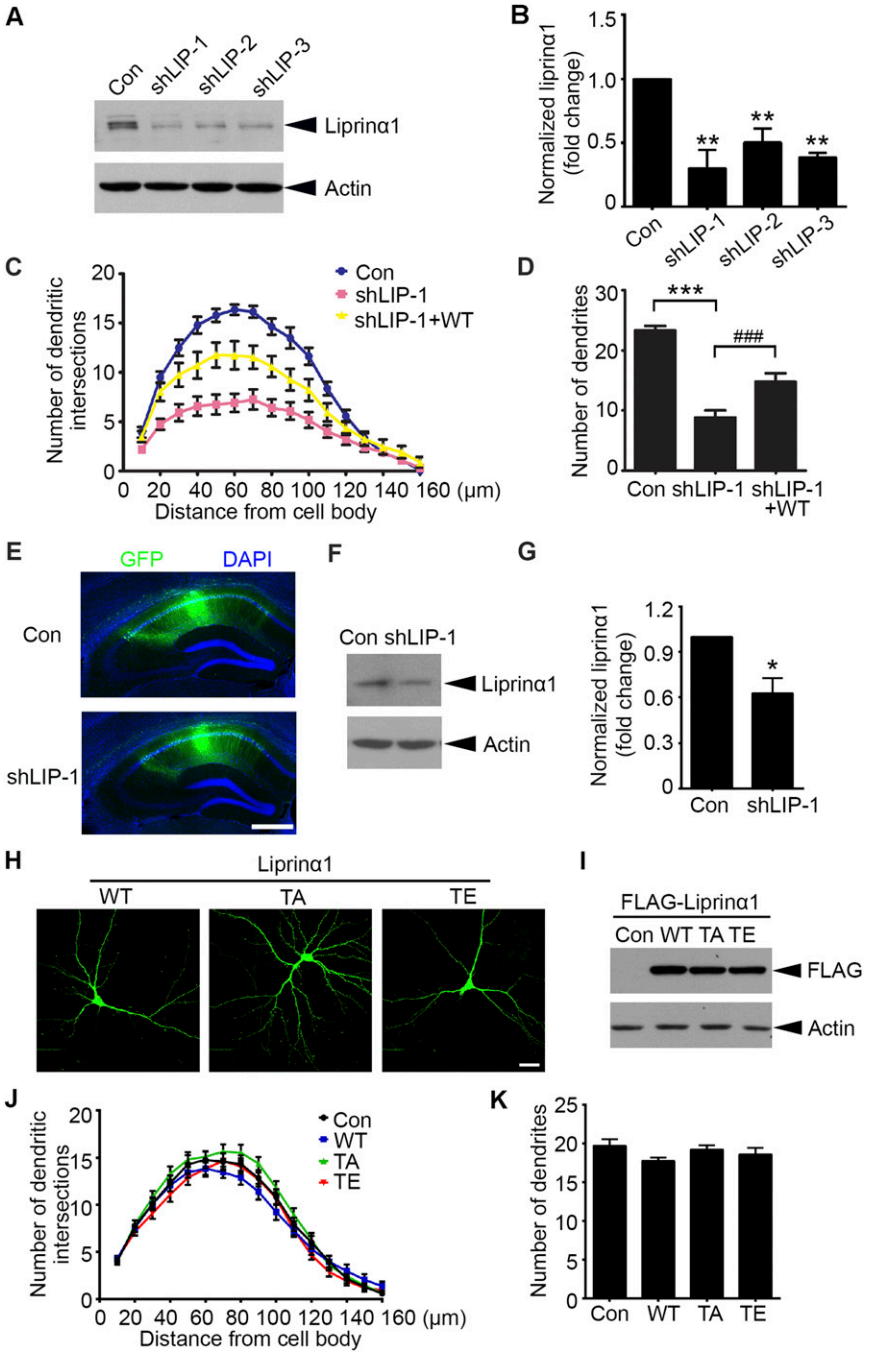


**Fig. S2.** Liprinα1, but not its phosphorylation status, is required for dendrite maintenance. (*A* and *B*) Western blot analysis of liprinα1 expression in cultured cortical neurons transfected with pSUPER vector as control (Con) and liprinα1 shRNAs. Protein level normalized to actin; $^{**}P < 0.01$ vs. Con, Student's *t* test; $n = 3$ independent experiments. (*C* and *D*) Liprinα1 knockdown resulted in significant dendritic defects, which were partially rescued by an RNAi-resistant human liprinα1 construct (WT). Cultured hippocampal neurons were transfected with the indicated plasmids at 12 DIV and cultured for 5 d. (*C*) The dendritic complexity of transfected neurons was analyzed by Sholl analysis. Knockdown of liprinα1 reduced the dendritic intersections 10–120 μm from somas compared with Con, which was partially rescued by WT. (*D*) Quantification of dendrites of transfected neurons. $^{***}P < 0.001$ vs. Con; $^{\#\#\#}P < 0.001$ vs. shLIP-1, one-way ANOVA with the Student–Newman–Keuls test; $n = 14$, 12, and 12 neurons for Con, shLIP-1, and shLIP-1+WT, respectively. (*E*–*G*) Liprinα1 expression was significantly reduced in the hippocampal CA1 region by lentiviral infection. (*E*) Representative images of mouse hippocampal slices infected by lentivirus containing shLIP-1 or GFP control (Con). Slices were stained with GFP (green) and DAPI (blue). (Scale bar: 500 μm.) (*F*) GFP-infected CA1 regions were dissected for Western blot analysis. (*G*) Quantification of liprinα1 expression. Normalized to actin; $^{*}P < 0.05$, Student's *t* test; $n = 4$ mice for each condition. (*H* and *I*) The expression levels of different liprinα1 constructs are comparable. (*H*) Immunostaining of overexpressed liprinα1 (green) in cultured neurons. (Scale bar: 25 μm.) (*I*) Western blot analysis of the overexpression levels of liprinα1 and its mutants in HEK293T cells. (*J* and *K*) Overexpression of TA or TE mutants of liprinα1 did not affect dendritic complexity compared with WT. Cultured hippocampal neurons were transfected with WT, TA, or TE liprinα1 or control pcDNA3 vector (Con) together with GFP at 12 DIV. Neurons were fixed and imaged at 17 DIV. $n = 21$, 24, 20, and 24 neurons for Con, WT, TA, and TE, respectively. All data are mean ± SEM.

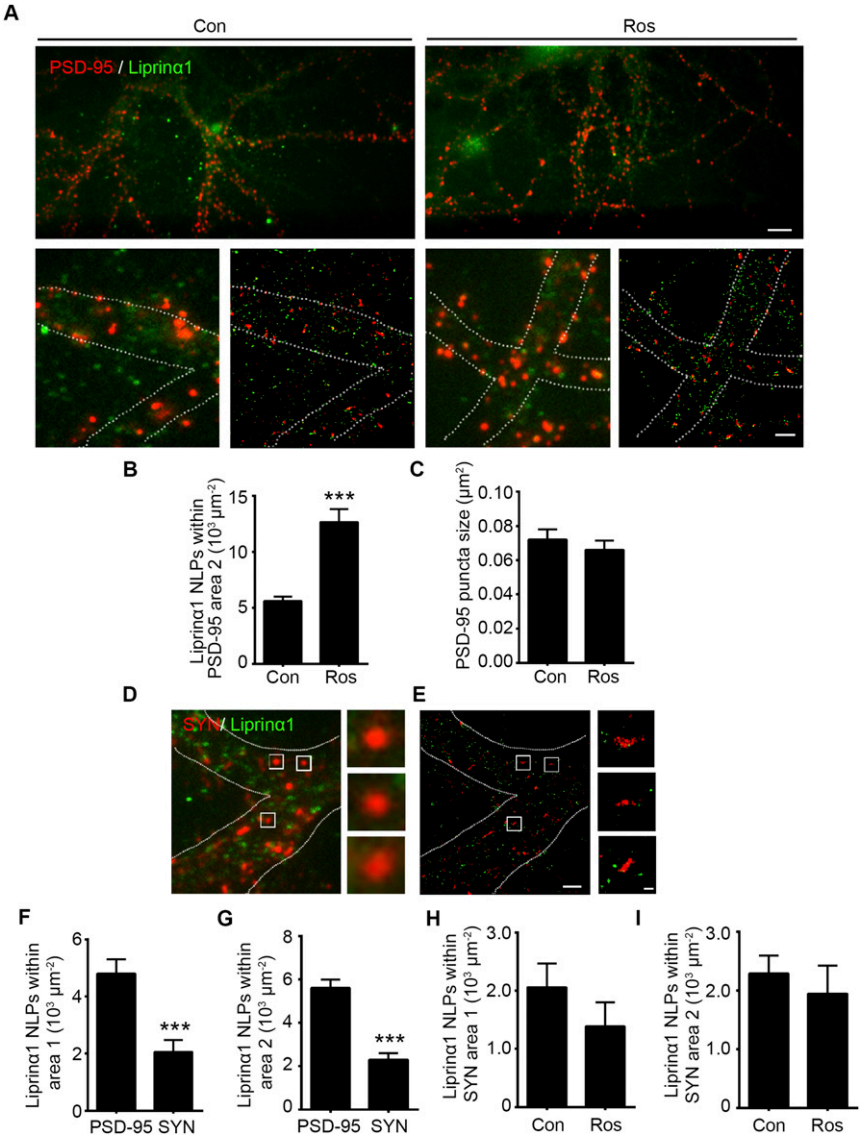


**Fig. S3.** Superresolution imaging showing that reduced liprinα1 phosphorylation increases the colocalization of liprinα1 with PSD-95 at postsynaptic regions. (*A–C*) Roscovitine (Ros) treatment increased liprinα1 localization density in the surrounding region of PSD-95 (area 2) but did not change PSD-95 puncta size. (A) Wide-field images of endogenous liprinα1 (green) and PSD-95 (red) (*Upper*: magnification, 40×, scale bar: 8 μm; *Lower*: magnification, 150×) and the corresponding STORM images (scale bar: 2 μm.) Neurons were treated with DMSO as a control (Con) or with Ros for 2 h and then stained with liprinα1 and PSD-95. (*B* and *C*) Quantification of the number of localization points (NLPs) of liprinα1 per $\mu m^2$ of area 2 and the size of PSD-95 puncta, respectively. ***$P < 0.001$, Student's *t* test; $n = 53$ and 51 synapses for Con and Ros, respectively. Data are mean ± SEM. (*D–G*) Liprinα1 was more enriched in the PSD-95–positive region than the synaptophysin (SYN)-positive region. (*D* and *E*) Low-magnification images and corresponding STORM images of liprinα1 (green) and SYN (red) (Scale bars: *Left*, 2 μm; *Right*, 200 nm.) (*F* and *G*) Quantification analysis of liprinα1 distribution density in PSD-95–positive and SYN-positive regions in area 1 (*F*) and area 2 (*G*). ***$P < 0.001$, Student's *t* test; $n = 53$ and 52 PSD-95– and SYN-positive regions, respectively. Data are mean ± SEM. (*H* and *I*) Quantification analysis showing that Ros treatment did not alter the density of liprinα1 localization in area 1 (*H*) or area 2 (*I*) of SYN. Student's *t* test; $n = 52$ and 34 regions for Con and Ros treatment, respectively.

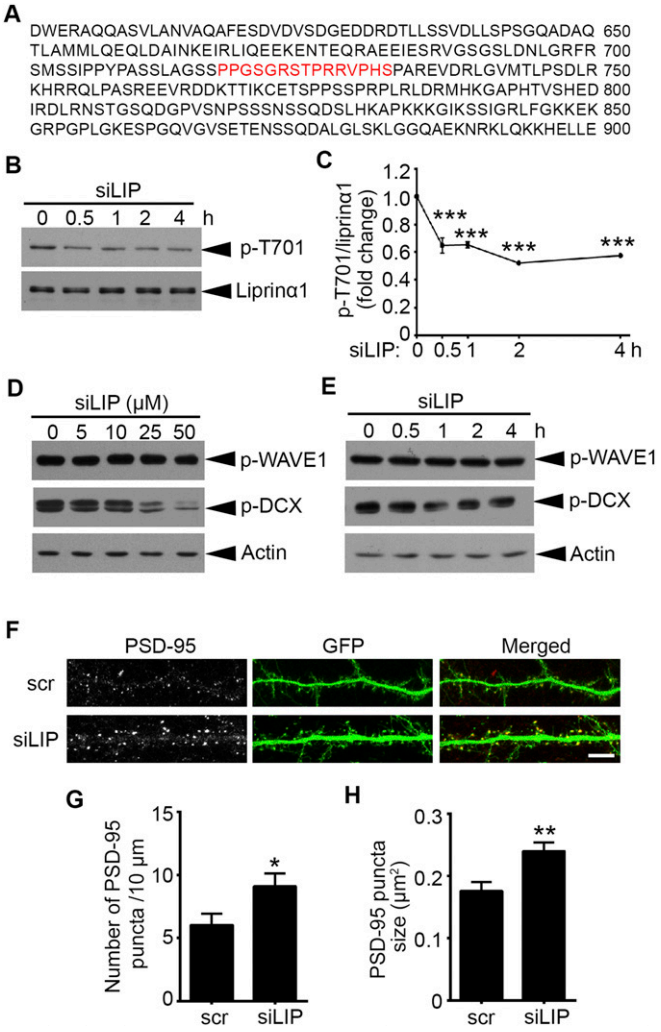


**Fig. S4.** Liprinα1 siLIP promotes synaptic localization of PSD-95. (*A*) The amino acid sequence of liprinα1 from 601 to 900, with the sequence of the siLIP highlighted in red. (*B* and *C*) Liprinα1 siLIP inhibited liprinα1 phosphorylation after treatment for 30 min to 4 h. (*B*) Western blot analysis of phosphorylated (p-T701) and total liprinα1. Cultured neurons were incubated with siLIP (10 μM) for the indicated period at 14 DIV. (*C*) Quantification of liprinα1 phosphorylation, normalized to liprinα1 protein level. ***$P < 0.001$, one-way ANOVA with the Student–Newman–Keuls test; $n = 3$ independent experiments. (*D* and *E*) Liprinα1 siLIP (≤10 μM) did not alter the levels of p-WAVE1 (Ser310) or p-DCX (Ser297). (*D*) Cultured neurons were incubated with siLIP for 2 h at the indicated dosages. (*E*) Cultured neurons were incubated with siLIP (10 μM) for the indicated periods. (*F–H*) Liprinα1 siLIP treatment increased the density and size of PSD-95 puncta at synaptic regions. Cultured hippocampal neurons were transfected with GFP at 12 DIV and treated with siLIP (10 μM, 30 min) at 19 DIV. (*F*) Representative images of PSD-95 localization along dendrites treated with scr or siLIP. (Scale bar: 10 μm.) (*G* and *H*) Quantification analysis of PSD-95 puncta density and size after treatment with scr (*G*) and siLIP (*H*). *$P < 0.05$; **$P < 0.01$, Student's *t* test; $n = 15$ and 12 dendrites for scr and siLIP, respectively. All data are mean ± SEM.